Preprints.org

Article

Cyclic Interannual Variation in Monsoon Onset and Rainfall in South-Central Arizona, U.S.A.

Frank W Reichenbacher [*] and William D. Peachey

Article

Cyclic Interannual Variation in Monsoon Onset and Rainfall in South-Central Arizona, U.S.A.

Frank W. Reichenbacher [1,*] and William D. Peachey [2]

[1] Desert Laboratory on Tumamoc Hill, University of Arizona, 1675 W Anklam Rd, Tucson, AZ, 85745; Orcid ID, 0000-0002-3381-4313

[2] Sonoran Science Solutions, 550 N. Avenida Venado, Tucson, AZ 85748; Orcid ID, 0000-0002-1497-3845

* Correspondence: frankr1@arizona.edu

Abstract: The North American Monsoon (NAM) in southern Arizona continues to be a topic of interest to many ecologists studying the triggers and characteristics of plant growth and reproduction in relation to the onset of the monsoon. The purpose of this article is to report interannual variation in the timing of NAM onset found while researching the phenology of Saguaro cactus (*Carnegiea gigantea*). Using a daily rainfall dataset from 33 stations located in Pima and Pinal Counties, Arizona, from 1990-2022, we analyzed monsoon onset, monsoon precipitation, annual precipitation, and the proportion of annual station precipitation received during the monsoon season. Onset was measured by the first day from 1 June to 30 September with precipitation ≥10 mm counted from the day of the vernal equinox of the year. Generalized Additive Models (GAMs) identified sinusoidal waves with period of 8.6 years and amplitudes of 14-29 days, providing frequency and amplitude estimates for Sinusoidal Regression Models (SRMs). Sinusoidal wave patterns found in the monsoon onset dataset are suggested in monsoon, annual, and proportion of monsoon in station-averaged annual precipitation although in and approximately mirror-image. These unexpected findings may have important implications for forecasters as well as ecologists interested in plant phenology.

Keywords: monsoon; North American Monsoon; precipitation; Sonoran Desert; Gulf of California; phenology; climate change; climatology; sea surface temperature; Sonora; Arizona

1. Introduction

1.1. Saguaro Phenology

The association of plant phenological response to the annual cycle of the North American Monsoon (NAM) has been the subject of much study by plant ecologists [1–3], but many details are not well characterized. Numerous plants of the Sonoran Desert of North America are partly or wholly dependent on NAM rainfall, but when does monsoon rainfall arrive at any one location? How does arrival timing vary over time and across plant generations? Or does it vary? Appearing as it does in the otherwise extremely hot summer months of June-September, the monsoon rains are vital to plant growth and reproduction [4–6]. One plant uniquely dependent on the monsoon is the saguaro cactus (*Carnegiea gigantea*) which flowers in April, produces fruits from May-June, and disperses seeds by mid-July [7–9]. Timing of seed dispersal anticipates the arrival of the first NAM rainfall events in July. Seed germination and seedling establishment requires sufficient NAM rainfalls to trigger germination and then provide moisture, elevated humidity, and lower temperatures to ensure seedling establishment. Seeds apparently do not survive for more than a few weeks after dispersal [10]. Many other species produce and disperse propagules immediately prior to NAM onset, however, as far as is known, at least a portion of those seeds survive the summer and persist in the soil for at least one more season [11,12]. Saguaro synchronization of phenological events with rainfall

events and extended periods of favorable climatic conditions is crucial for reproduction. Phenological synchrony with climatic cues is an area of intense ecological research [13–16].

1.2. North American Monsoon

The synoptic NAM rainfall system emerges from seasonal variations in latitudinal migrations of the Intertropical Convergence Zone (ITCZ, [17,18]). As the ITCZ migrates northward from the equator toward Central America in the northern hemisphere spring, winds along the Pacific coast of Central America and Mexico shift from westerly to southerly transporting increasing quantities of low-level moisture north and northwest along the Mexican coast and eventually entering into Arizona [19,20]. The ITCZ linkage is a relatively recent interpretation made possible primarily through the analysis of global precipitation revealed by satellite sensors [21]. Over the past 30 years, climatologists have achieved considerable success in explaining the causes and mechanisms driving the NAM phenomenon. In particular, the North American Monsoon Experiment (NAME) project of the early 2000s [22]. In addition to compiling impressive datasets from a variety of sensor sources, the NAME researchers worked hard to resolve disagreements regarding the source(s) of NAM moisture and the role of the Gulf of California (GoC) as a mechanistic component of the NAM system [23,24].

Previous research found some indication that the onset and retreat of monsoon weather has changed, perhaps reflecting changes in the ITCZ. Arias, et al. [25] found that the NAM season has shortened due to earlier retreat while the SAM (South American Monsoon) has lengthened by a correlated amount. Ashfaq, et al. [26], using multiple regional projections, predicted broad monsoon onset delays and less overall precipitation, which, if realized, could have significant effects on saguaro phenology.

1.3. Defining Monsoon Onset

The goal of this study was to determine whether saguaro reproductive phenology is synchronized with important climatic events, particularly regarding the timing of seed dispersal and the onset of the monsoon. This first required an objective determination of the date of monsoon onset for a period long enough to discern trends and patterns. We then sought monsoon onset criteria that could be identified from a daily rainfall record, available for many stations in our area from online sources, would yield a single day date, and considered the needs of the plants of the desert. Several methods for identifying monsoon onset were reviewed.

Brenner [27] noted a variety of measurements to indicate that the northward surge of the seasonal maritime airmass from GoC to Arizona has begun, including hourly observations of temperature, dew point, and pressure. In the 1980s meteorologists associated with the U.S. National Weather Forecasting Offices in Phoenix and Tucson began to rely on dew point temperature criteria [28]. Bombardi, et al. [29] catalogued detection methods or criteria from 32 published references, about half of which were solely or partly based on precipitation criteria.

Bowers, et al. [30] found that precipitation amounts triggering seedling emergence in 15 perennial plant species ranged from 17-36 mm. This threshold is higher than necessary to trigger flowering in established perennial plants. Bowers and Dimmitt [2] found that a rainfall event of as little as 9 mm was sufficient to trigger flowering in triangleleaf bursage (*Ambrosia deltoidea*) and Bowers [8] found that as little as 5 mm of rain triggered flowering in the saguaro cactus. Therefore, for the purposes of this analysis it was determined that the first single-day rainfall of ≥10 mm, from 1 June to 30 September, would be used. This amount is large enough to potentially trigger plant growth and almost every weather station in the dataset recorded on at least one day at some point during the NAM season.

As plant ecologists, we are interested in the influence of environmental signals on phenological triggers and how this might affect the viability of the saguaro cactus and many other plant species. During investigations of the relationship between saguaro phenology and climate, we found interesting patterns in NAM early and late onsets. The purpose of this article is to report the results

of our preliminary analyses suggesting previously unreported cyclic interannual variation of in NAM onset and precipitation in south-central Arizona. In subsequent publications we plan to present analyses of the influence of changes in the date of onset of NAM on saguaro phenology.

2. Methods

Precipitation Dataset

The monsoon season was considered to include the period from 1 June to 30 September and monsoon onset was defined as the first day from 1 June to 30 September with single-day rainfall of ≥10 mm. Our primary dataset was constructed with daily precipitation gathered from the Pima County, Arizona, ALERT network of remote reporting rain gauges [31], the Global Historical Climatology Network (GHCN-Daily [32,33]) and Remote Automated Weather Stations (RAWS [34]), most with records from 1990-2022 (Table 1, Figure 1). Data for the full 33-year period from 1990-2022 were obtained from 22 of 33 weather stations. Years of record for the remaining 11 stations ranged from 22 to 32 years.
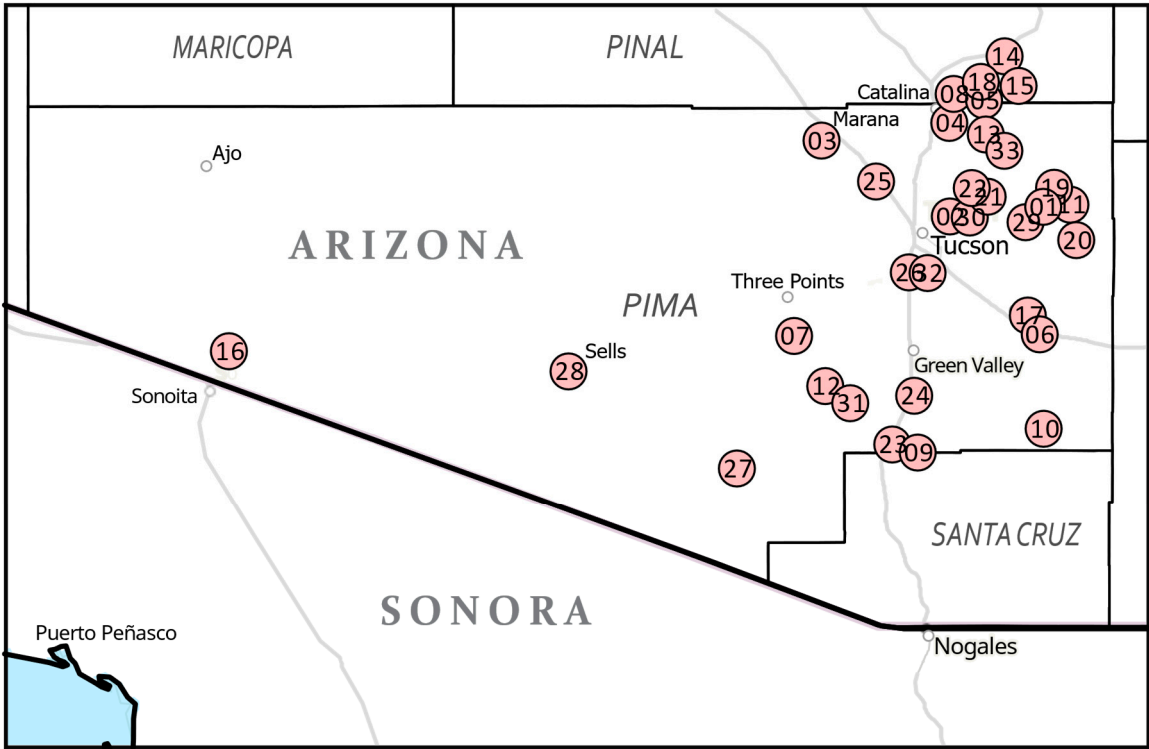

Figure 1. Map of the locations of the 33 weather stations used in this analysis, Pima and Pinal counties, Arizona. See Table 1 for station metadata.

Table 1. List of 33 weather stations sorted by elevation. Stations were chosen for length of record and elevational representation. Year with >10 missing daily rainfall totals during the 1 June-30 September sample period were omitted. Station record period listed here is that used for this analysis.

	Station Name	Station ID	Network	Period of Record Used	Elev. (m)	Latitude	Longitude
1	Alamo Tank	2080	Pima Co. ALERT[1]	1990-2022	1212	32.2797	-110.6350
2	Alamo Wash/Glenn St	2370	Pima Co. ALERT[1]	1990-2008, 2010-2021	745	32.2587	-110.8841
3	Avra Valley Air Park/Santa Cruz R	6110	Pima Co. ALERT[1]	1990-2000, 2002-2022	606	32.4290	-111.2251
4	Catalina State Park	1070	Pima Co. ALERT[1]	1991-2021	825	32.4235	-110.9161
5	Cherry Tank	1050	Pima Co. ALERT[1]	1990-2021	1232	32.5181	-110.8370
6	Davidson Canyon	4310	Pima Co. ALERT[1]	1990-2022	1057	31.9936	-110.6451
7	Diamond Bell Ranch	6410	Pima Co. ALERT[1]	1990-1999, 2001-2022	994	31.9897	-111.2972
8	Dodge Tank	1040	Pima Co. ALERT[1]	1990-2020	1013	32.5119	-110.8642
9	Elephant Head	6350	Pima Co. ALERT[1]	1990-2022	1062	31.7250	-110.9678
10	Empire	021205	RAWS[4]	1990-2011, 2013-2016, 2018-2022	1393	31.7806	-110.6347
11	Italian Trap	2030	Pima Co. ALERT[1]	1990, 1992-2022	1254	32.2853	-110.5636

12	Keystone Peak	6310	Pima Co. ALERT[1]	1990-2021	1877	31.8769	-111.2150
13	Mount Lemmon	1090	Pima Co. ALERT[1]	1990-2022	2790	32.4427	-110.7885
14	Oracle R.S. CDO	1020	Pima Co. ALERT[1]	1990-2019, 2021	1436	32.5855	-110.7868
15	Oracle Ridge	1030	Pima Co. ALERT[1]	1990-2021	1963	32.5328	-110.7562
16	Organ Pipe Cactus NM	USC00026132	NCEI[2]	1990-2001, 2003-2022	512	31.9555	-112.8002
17	Pantano Vail	4250	Pima Co. ALERT[1]	1990, 1992-2019, 2022	982	32.0361	-110.6767
18	Pig Springs	1060	Pima Co. ALERT[1]	1990-2022	1463	32.5261	-110.7948
19	Ranch Rd	2050	Pima Co. ALERT[1]	1990-1993, 1995-2022	1312	32.3103	-110.6061
20	Rincon	021207	RAWS[4]	1995-1999, 2002-2022	2482	32.2056	-110.5481
21	Sabino Dam	2160	Pima Co. ALERT[1]	1991-2022	834	32.3147	-110.8106
22	Saguaro	021202	RAWS[4]	2002-2022	890	32.3167	-110.8133
23	Santa Cruz R/Canoa Ranch	6060	Pima Co. ALERT[1]	1990-2022	917	31.7447	-111.0372
24	Santa Cruz R/Continental Rd	6050	Pima Co. ALERT[1]	1990-2021	866	31.8542	-110.9792
25	Santa Cruz R/Ina Rd	6020	Pima Co. ALERT[1]	1990-2000, 2002-2022	659	32.3372	-111.0800
26	Santa Cruz R/Valencia Rd	6040	Pima Co. ALERT[1]	1990-1996, 1998-2021	752	32.1342	-110.9919
27	Sasabe	021206	RAWS[4]	1992-2022	1007	31.6908	-111.4500
28	Sells	021209	RAWS[4]	2005-2006, 2008-2009, 2011-2022	714	31.9100	-111.8975
29	Tanque Verde Guest Ranch	2090	Pima Co. ALERT[1]	1990-1992,1994-2008, 2010-2021	832	32.2458	-110.6827
30	Tanque Verde Sabino Bridge	2120	Pima Co. ALERT[1]	1990-2000, 2001-2010, 2011-2022	756	32.2653	-110.8414
31	Tinaja Ranch	6320	Pima Co. ALERT[1]	1990, 1992, 1994-2022	1194	31.8381	-111.1483
32	Tucson Int'l Airport	USW00023160	NCEI[2]	1990-2022	778	32.1315	-110.9564
33	White Tail	2150	Pima Co. ALERT[1]	1990-1992, 1994-2022	2493	32.4136	-110.7319

[1] Pima County Flood Control District, https://alertmap.rfcd.pima.gov/gmap/gmap.html. [2] Western Regional Climate Data Center, https://raws.dri.edu/wraws/azF.html . [3] National Centers for Environmental Information, GHCND, https://www.ncei.noaa.gov/products/land-based-station/global-historical-climatology-network-daily.

Variables of interest, which will be referred to as below for the remainder of this paper, extracted from the precipitation dataset included:

- Day-of-year (***DOY onset***) of the first one-day rainfall events of ≥10 mm from 1 June -30 Sept., 1990-2022. To mitigate possible calendar bias in our method of determining the day-of year of monsoon onset the dates of monsoon onset were counted from the date of the vernal equinox of that year instead of from the first of the year. The date of the vernal equinoxes was obtained from the seasons calculator at timeanddate.com for Tucson, Arizona [35].
- Total monsoon rainfall (***MR***, mm, 1 June- 30 Sept.).
- Total annual rainfall (***AR***, mm).
- Proportion of mean annual station rainfall falling from 1 June – 30 Sept (***PAR***). Each year value in this vector is calculated as the difference between monsoon rainfall of the year and station mean annual rainfall across years.

Of the 33 stations used in the analysis all but three were within a 65 km radius of downtown Tucson, representing 2278 m of elevation from 512 m, at the Organ Pipe Cactus National Monument Headquarters, to 2790 m at the summit of Mt. Lemmon, Santa Catalina Mts. The geographical area covered by the selected stations, 17225 km², was chosen mainly because of the predominance of the Pima County ALERT network in the dataset within the range of the saguaro, but with the addition of stations with sufficient periods of record to sample the region west and south of Tucson, and a few RAWS stations to fill in elevation gaps. The Spatial Autocorrelation tool in ArcGIS Pro v. 3.2 [36] was used to determine whether the 33-year station means of the day after the vernal equinox of the first day rainfall ≥10 mm was influenced by proximity. The input data were weighted to include station elevation (z coordinates) calculated using inverse Euclidean distances.

When required for particular analyses, missing values were filled using the imputeTS package moving average algorithm (R package, ImputeTS [37]). On the few occasions with no rainfall ≥10 mm was recorded during that period (17 of 1,049 DOY records) the highest one-day amount during the period was substituted. The substitution procedure may have led to a slight bias to later DOY onset as at some of these stations the highest amount recorded from 1 June-30 Sept. occurred very late (as late as 30 September).

Least-squares linear regression models (LRMs) were created for the four variables time series listed above as well as (1) DOY onset and MR on elevation, (3-5) MR, AR, and PAR with DOY onset as predictor using base R ([38]). To investigate correlations between stations, Spearman's Rank statistics for the 33 stations with respect to DOY onset were calculated, also in base R ([38]). Autocorrelation function plots and residuals plots were created for the DOY onset time series using

the R forecast package [39]. Normality was investigated using probability density and QQ plots and Shapiro-Wilk tests of the per-station onset time series base R [38]. The time series of the four key variables listed above were tested using multivariate (multi-site) Mann-Kendall monotonic trend (R package trend, [40]). Cross-correlation tests were run with MR, AR, and PAR time series as response and DOY onset as the predictor using base R [38].

Patterns in scatterplots for each variable (DOY onset, MR, AR, PAR) suggested non-linearity that generalized additive models (GAMs) might elucidate. GAMs are widely employed in many fields when non-parametric analyses and relaxation of normality assumptions are desired [41–43]. Fit curves with basis dimensions set to k = 10 were generated from GAMs developed in R using the MGCV package [44] for the four variables. The results   were useful in estimating sinusoidal wave periods and coefficient starting points for sinusoidal regression models (SRMs) using the MATLAB Curve Fitter tool [45] of the form:

$$f(y)=a \sin(bx+c)+d$$

where y = DOY onset, MR, AR, or PAR, a = amplitude, x= year, b = change in period, c = horizontal shift, and d = vertical shift (calculated in base R [38].

3. Results & Discussion

3.1. Effect of Elevation on DOY Onset & Precipitation

In our NAM study area, orography strongly influences precipitation and at most sites there is a significant positive relationship between monsoon precipitation and elevation [46,47]. Figure 2 illustrates this with LRM of mean station MR on station elevation (R^2=0.891, p-value=<.001). In addition, DOY onset data regressed on elevation (Figure 3) also suggested a positive relationship (R^2=0.540, p-value=<.001). Thus, an early onset is associated with higher MR along the elevational gradient. Higher elevation sites generally have a greater probability of rainfall ≥10 mm on any day (both from the increased frequency of rainfall events and from the greater precipitation received from each event) and are, therefore, more likely to achieve our rainfall threshold (≥10 mm/day) sooner rather than later in any arbitrarily chosen period, including the monsoon season. The association of earlier onset with increasing elevation in our region is not unexpected, however, it is surprising that our DOY onset data, mixing untransformed gauge data from a broad elevational range should nevertheless exhibit the coherent cyclic pattern of interannual variation described in the next section. Early in our analysis we removed the effects of elevation on DOY onset variance, however, this had almost no effect on subsequent analyses and was not pursued. The positive correlation between monsoon precipitation and elevation observed in our gauge ensemble was not observed in other areas, including some relatively close by, such as northwestern Mexico, where distance from the Pacific Ocean coastline and the Sierra Madre Occidental are more reliable predictors ([48,49].
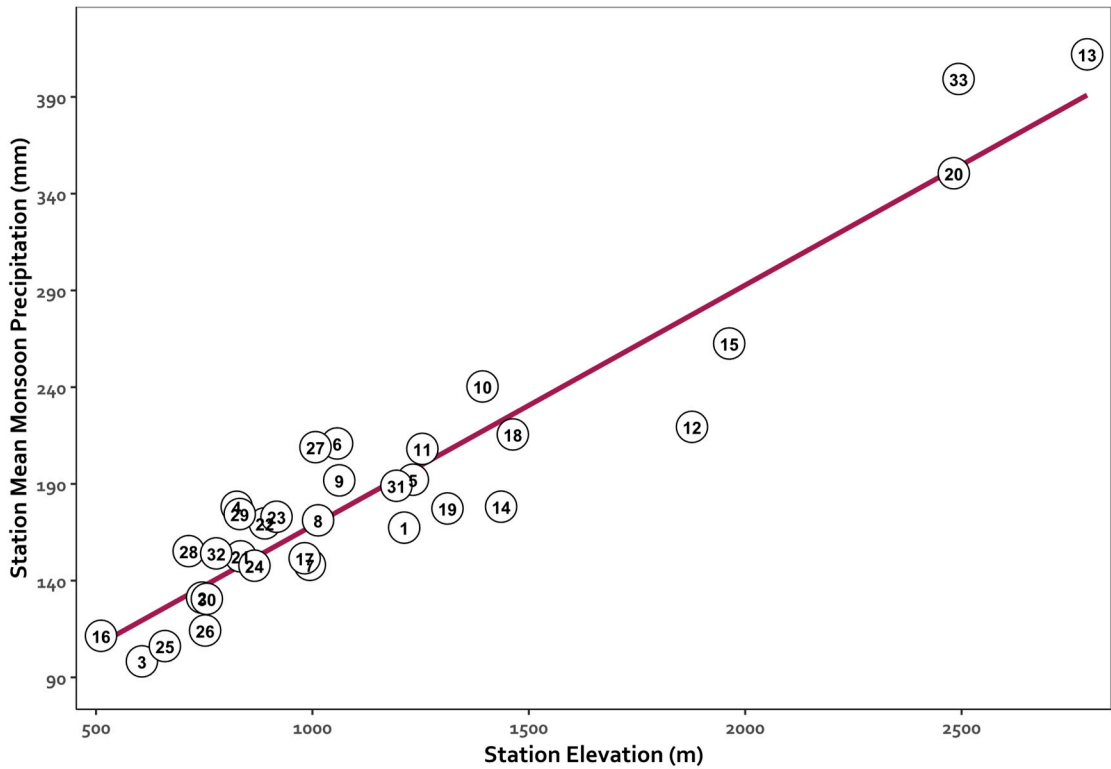
Figure 2. Linear regression (violet line) of mean monsoon precipitation by station (pink circles with numbers refer to Table 1) on station elevation, 1990-2022 for 33 meteorological stations in Pima and Pinal Counties, Arizona (R^2=0.891, p-value=<.001.
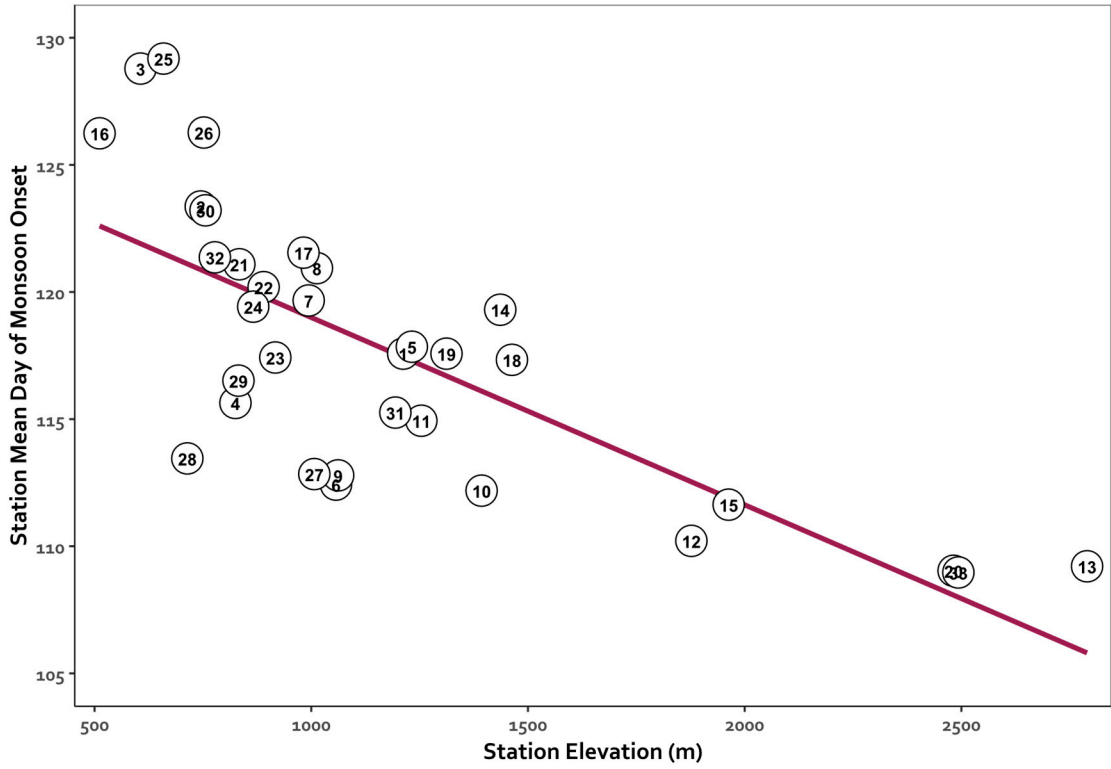

Figure 3. Linear regression (violet line) of day of year monsoon onset by station (pink circles with numbers refer to Table 1) on station elevation, 1990-2022 for 33 meteorological stations in Pima and Pinal Counties, Arizona (R^2=0. 0.540, p-value=<.001).

3.2. Monsoon Day-of-Year Onset

Table 2 lists the 33 weather stations, mean DOY onset, MR, AR, and PAR for each station. (Note that DOY onset is counted from the day of vernal equinox of each year). The mean DOY onset of all 33 stations from 1990-2022 was 16 July (min.=20 June, max.=8 August), 117.6 days from the vernal equinox date (usually March 20). Figure 4 is a correlation matrix (Spearman's Rank) of DOY onset for the 33 weather stations listed in Table 2 sorted by elevation. Of the 528 correlations, 346 are significant (p-value ≤0.05), all are positive correlations, and all but seven of those are moderately correlated ($\varrho <$ 0.75). The mean value of the 528 correlation coefficients is 0.40. The ArcGIS Pro v. 3.2 Spatial Autocorrelation tool [36] of DOY onset means for each station produced Moran's I = -0.005, z = 0.318, p-value = 0.750, indicating not different from random. ArcGIS Pro v. 3.2 Spatial Nearest Neighbor tool [36] indicates spatial distribution not different from random (p-value=0.654) and the mean between-station distance is 13.5 km. At nearest neighbor distances of 17.0 km and 11.3 km Gebremichael, et al. [50], Mascaro, et al. [51], respectively, also found low between-station correlations.
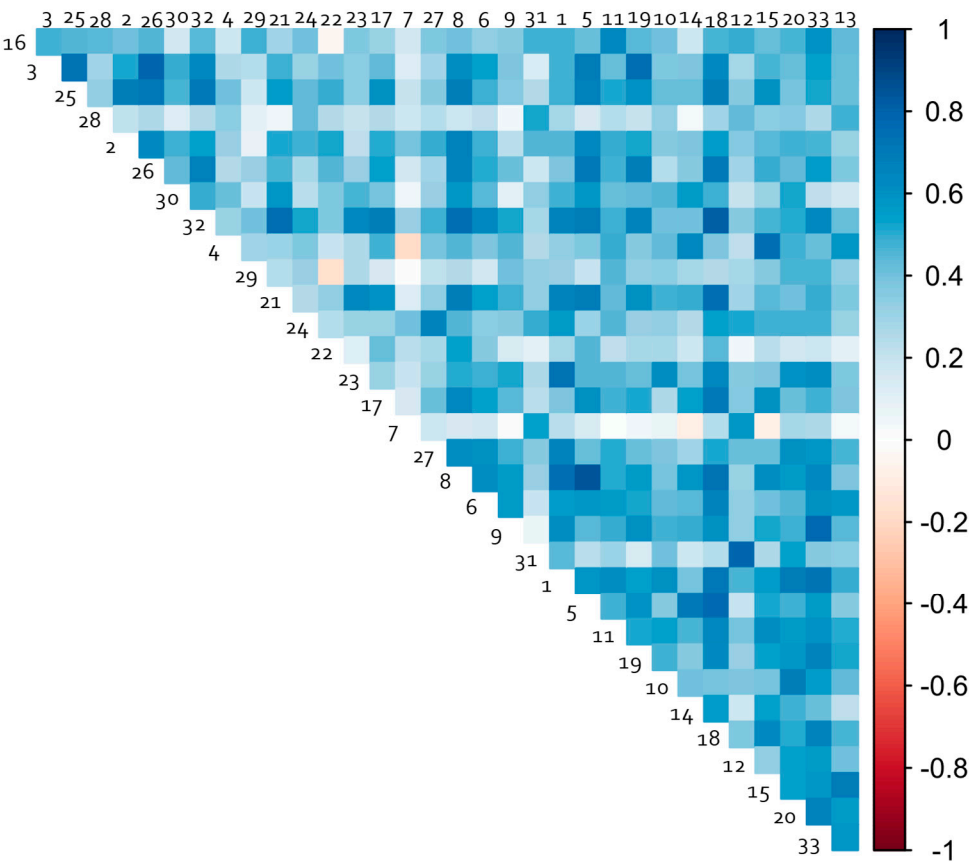

Figure 4. Correlation plot of 33 weather stations, DOY onset ordered by elevation from left-right and top-bottom. Numbers refer to stations in Table 1. Out of 528 possible correlations (Spearman's rank), 346 were significant (ρ>0.50, p-value <0.05), all positive.

Table 2. Mean day of monsoon onset (DOY onset), Mean rainfall (MR), Mean annual rainfall (AR), and monsoon proportion of annual rainfall (PAR) for 33 weather stations in Pima and Pinal Counties, Arizona, 1990-2022. Note that DOY onset is counted from the day of vernal equinox of each year.

	Station	DOY onset	Monsoon Rainfall (MR, mm)	Annual Rainfall (AR, mm)	Monsoon Proportion of Annual Rainfall (PAR
1	Alamo Tank	117.58	167.40	345.44	0.48
2	Alamo Wash below Glenn St	123.36	131.23	244.69	0.54
3	Avra Valley Air Park - Santa Cruz Basin	128.79	98.29	199.32	0.49
4	Catalina State Park	115.64	178.18	348.69	0.51
5	Cherry Spring	117.85	192.16	379.87	0.51
6	Davidson Canyon	112.42	210.89	360.39	0.59
7	Diamond Bell	119.67	148.17	249.32	0.59
8	Dodge Tank	120.94	171.17	343.37	0.50
9	Elephant Head	112.79	191.82	306.42	0.63
10	Empire	112.19	240.36	359.13	0.67
11	Italian Trap	114.94	208.11	393.66	0.53
12	Keystone Peak	110.21	219.48	328.28	0.67
13	Mount Lemmon	109.21	411.99	809.18	0.51
14	Oracle Ranger Stn at Canada del Oro	119.30	178.23	356.17	0.50
15	Oracle Ridge	111.64	262.55	480.58	0.55
16	Organ Pipe Cactus NM	126.24	111.49	234.81	0.47
17	Pantano Vail	121.55	151.58	244.53	0.62
18	Pig Springs	117.33	215.57	451.81	0.48
19	Ranch Road	117.58	177.29	360.22	0.49
20	Rincon	109.69	349.48	574.48	0.61
21	Sabino Dam	121.47	149.06	302.59	0.49
22	Saguaro	120.19	169.61	309.14	0.55
23	Santa Cruz River at Canoa Ranch	117.42	173.03	271.15	0.64
24	Santa Cruz River at Continental Rd	119.42	147.73	243.46	0.61
25	Santa Cruz River at Ina Road	129.18	106.19	204.48	0.52
26	Santa Cruz River at Valencia Road	126.27	114.23	208.66	0.55
27	Sasabe	112.40	210.67	334.04	0.63
28	Sells	113.45	155.26	251.99	0.62
29	Tanque Verde Guest Ranch	115.91	174.43	328.58	0.53
30	Tanque Verde Sabino Bridge	123.21	130.59	240.29	0.54
31	Tinaja Ranch	115.26	189.03	310.90	0.61
32	Tucson Int'l Airport	121.36	154.09	273.47	0.56
33	White Tail	108.97	399.27	758.54	0.53
	Grand Total/Mean	117.58	167.40	345.44	0.48

Indeed, although DOY onset is associated with elevation, visual inspection of Figure 4 suggests that sites at similar elevations do not appear more likely to be correlated with respect to each other. Even very close stations may exhibit low correlations. Sabino Dam and Saguaro (Table 1), separated by 337 m horizontal and 56 m elevation, are correlated with ρ = 0.385, while Organ Pipe Cactus National Monument and Mt. Lemmon, ρ = 0.431, are separated by 197 km and 2274 m elevation.

The partial independence of monsoon rainfall gauge readings in the desert and semidesert lands of southwestern North America has long been recognized ([52]), which is how our gauge-based network is treated for the purpose of this analysis.

Figure 5 depicts the probability density plot and normal curve of the DOY onset dataset (all 33 stations, 1990-2022, 1,049 data points) showing a left-skew reflecting the fewer, but more tightly clustered early onset DOY onsets characteristic of the sinusoidal wave troughs. Shapiro-Wilk tests of the per-station onset time series indicate non-normality in the onset day for two-thirds of stations and non-normality of onset distribution when the data are tested per-year in every year from 1990-2022. Monsoon DOY onset is therefore likely to be normally distributed for the station when accumulated over time, but non-normal for DOY onset for any given year across the stations.

We suggest that the skewed DOY onset timing is the result of at least two conditions: (1) an imbalanced effect of the fewer early DOY onset years that exhibit less variance as discussed in the next section, and (2) the beginning date of the monsoon was set at 1 June while the end date was set at 30 September, a span of 122 days. Mean DOY onset date was 16 July, 46 days from 1 June and 76 days from 30 September. There is more time after the mean DOY onset date for stations to achieve the ≥10 mm criterion than before.
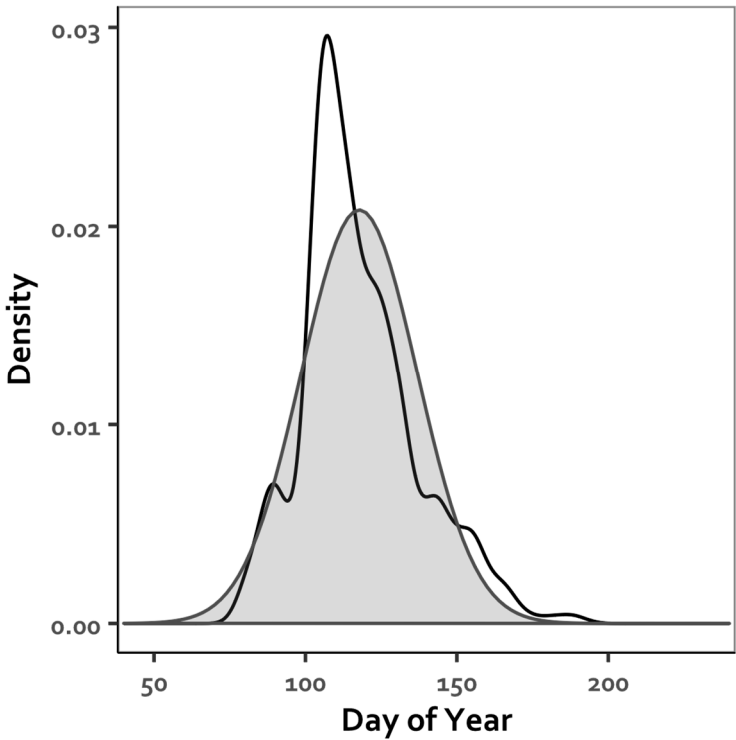
Figure 5. Probability density (white) and normal curve (gray) of the DOY onset dataset (all 33 stations, 1990-2022, 1,047 data points). Note that DOY onset is counted from the day of vernal equinox of each year.

3.3. GAMs, LRMs, and SRMs

Figures 6–9 present scatterplots, GAMs, LRMs, and SRMs for DOY onset, MR, AR, and PAR (1 June-30 September) for the 33 weather stations listed in Table 2. Summary statistics are listed in Table 3 and crest-trough periods and amplitudes derived from the GAM curves are listed in Table 4.

Table 3. Results of generalized additive models (GAM), linear regressions (LRM), sinusoidal regressions (SRM), and multivariate MK Test (MK trend, R package trend, mult.mk.test, tau not a product) on DOY onset, MR, AR, and PAR for 33 weather stations in Pima and Pinal Counties, Arizona, 1990-2022.

| Model/Test	Response	Statistic	Value	P-value
GAM		Deviance explained	19.1%	
LRM	DOY Onset	R^2	0.032	<0.001
SRM		R^2	0.176	<0.001
MK Trend				0.511
GAM		Deviance explained	13.3%	<0.001
LRM	Monsoon Rainfall	R^2	0.022	<0.001
SRM		R^2	0.084	
MK Trend				0.654
GAM		Deviance explained	5.4%	<0.001
LRM	Annual Rainfall	R^2	<0.001	0.830
SRM		R^2	0.038	
MK Trend				0.861
GAM		Deviance explained	21.4%	<0.001
LRM	Monsoon Rainfall Proportion of	R^2	0.025	<0.001
SRM	Annual	R^2	0.174	
MK Trend				0.052
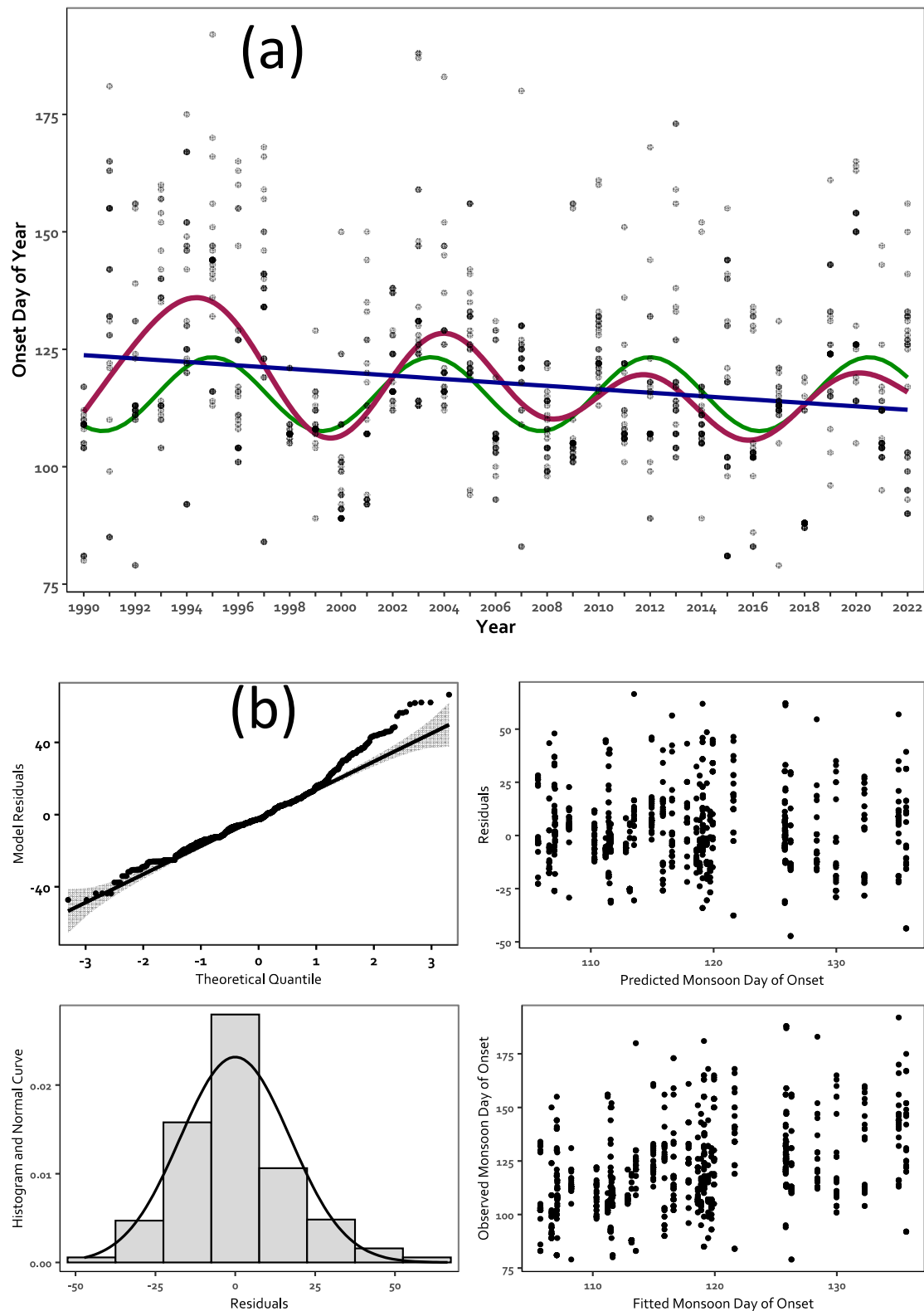
Figure 6. a. Scatterplot, LRM, GAM, and SRM, DOY monsoon onset, 33 stations, 1990-2022 -- gray dots=individual station scores, dark blue line=LRM, R²=0.032, p-value=<0.001, violet curve=GAM onset, deviance explained=19.1%, p-value=<0.001; green curve=SRM, R²=0.176. b. Diagnostic visuals -- QQ plot, plot of residuals, histogram of residuals, and observed vs. predicted scores. Note that DOY onset is counted from the day of vernal equinox of each year.
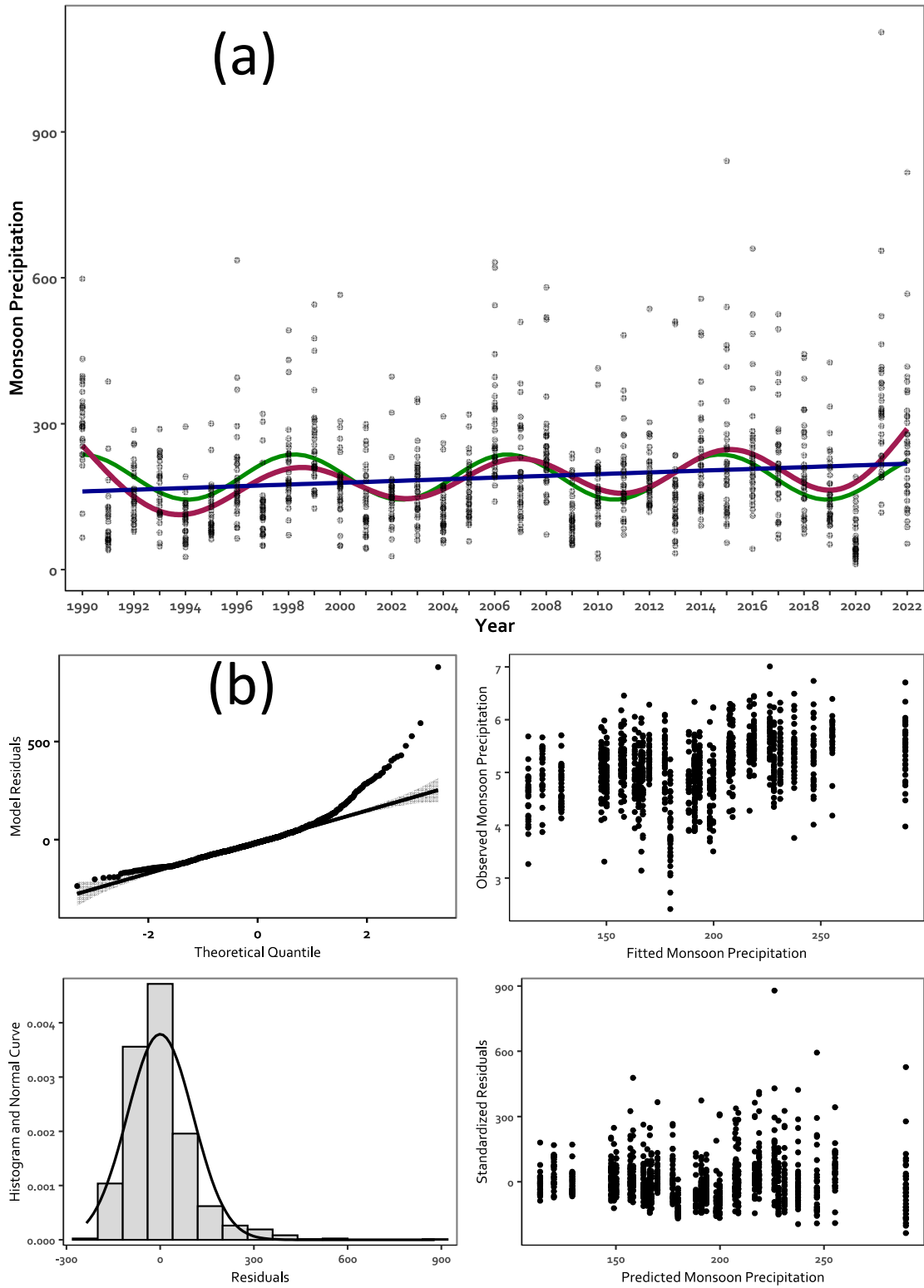
Figure 7. a. Scatterplot, LRM, GAM, and SRM, of monsoon precipitation (MR), 33 stations, 1990-2022 -- gray dots=individual station scores, dark blue line=LRM, R^2=0.022, p-value=<0.001, violet curve=GAM, deviance=13.3%, p-value=<0.001; green curve=SRM, R^2=0.084. b. Diagnostic visuals -- QQ plot, plot of residuals, histogram of residuals, and observed vs. predicted scores.
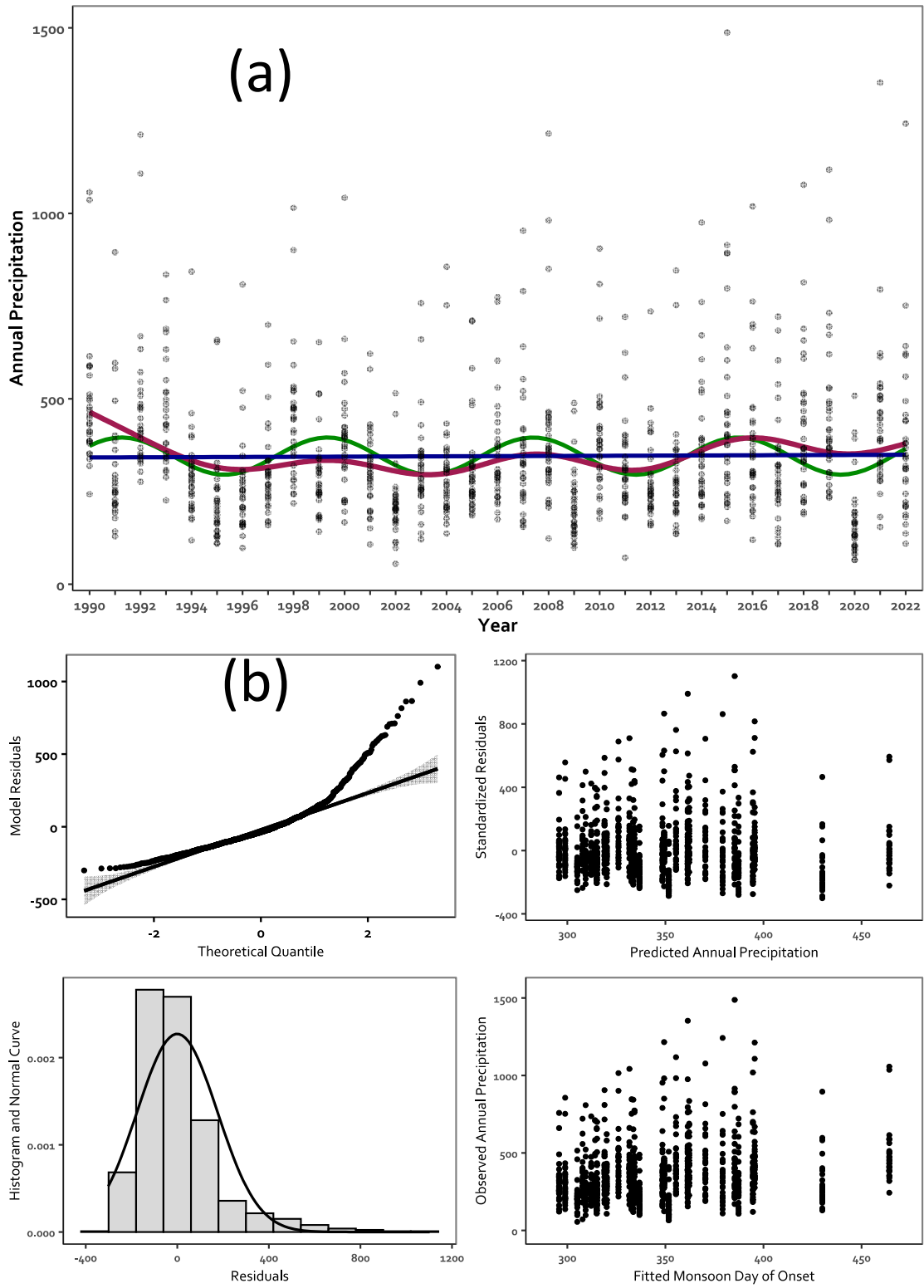
Figure 8. a. Scatterplot, LRM, GAM, and SRM, annual precipitation (AR), 33 stations, 1990-2022 -- gray dots=individual station scores, dark blue line=LRM, R²=<0.001, p-value=0.830 violet curve=GAM, monsoon precipitation, deviance=5.4%, p-value=<0.001; green curve=SRM, R²=0.038. b. Diagnostic visuals -- QQ plot, plot of residuals, histogram of residuals, and observed vs. predicted scores.
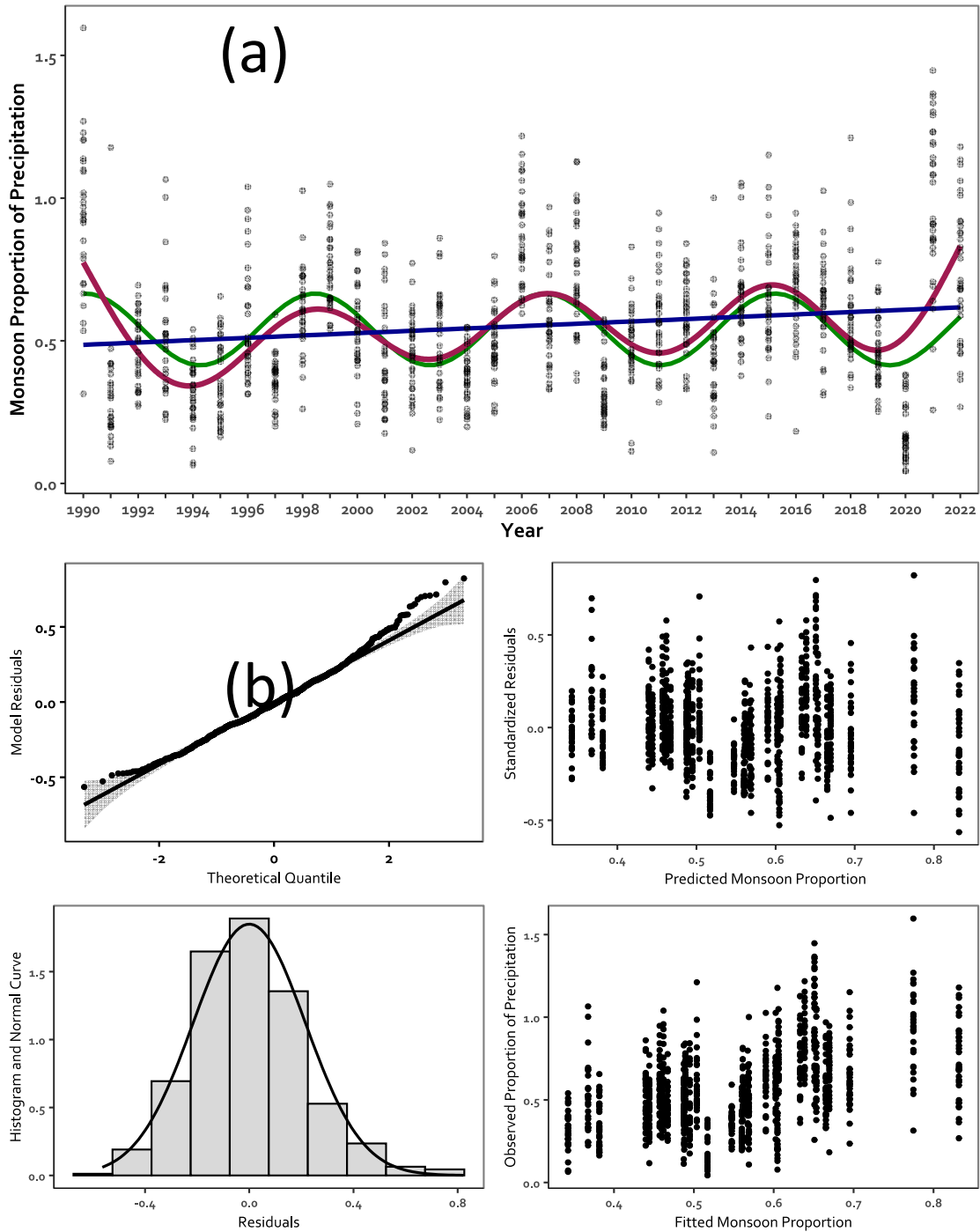
Figure 9. a. Scatterplot, LRM, GAM, and SRM, monsoon proportion of station annual rainfall (PAR), 33 stations, 1990-2022 -- gray dots=individual station scores, dark blue line=LRM, R²=0.025, p-value=<0.001, violet curve=GAM, monsoon precipitation, deviance=21.4%, p-value=<0.001; green curve=SRM, R²=0.174. b. Diagnostic visuals -- QQ plot, plot of residuals, histogram of residuals, and observed vs. predicted scores.

Table 4. Sinusoidal curve, crest and trough dates and crest-crest periods, 1990-2022. Calculated from the GAM outputs (Figs. 7-10). Note that DOY onset is counted from the day of vernal equinox of each year; calendar date is shown here.

Variable	Crest	Trough	Amplitude (Crest-Trough)	Period, Mean Crest->Crest
DOY onset	1994/05/09	1999/08/07	30 days	3140 days

	2004/01/06	2008/03/28	18 days	8.6 years
	2011/10/05	2015/11/09	14 days	
	2020/02/22			
MR	1998/07/06	1993/10/11	97 mm	
	2006/12/17	2002/08/10	82 mm	3039 days
	2015/02/25	2010/12/05	90 mm	8.3 years
		2018/12/29	89.667	
AR	1999/05/06	1995/12/14	39 mm	
	2007/07/15	2003/04/01	44 mm	3050 days
	2016/01/18	2011/04/01	43 mm	8.4 years
		2019/10/05		
PAR	1998/09/14	1993/11/03	27 pct	
	2006/12/17	2002/08/10	23 pct	2969 days
	2014/12/17	2010/12/29	24 pct	8.1 years
		2018/12/29		

Notwithstanding the low p-values listed in Table 3 for the linear regressions of DOY onset, MR, AR, and PAR shown in Figures 6–9, low R^2 values indicate very little variance, if any, is explained. This was due, at least in part, to the confounding effects of the sinusoidal wave pattern. Tests of the time series with multivariate (multi-site) Mann-Kendall monotonic trend (R package, trend, [40]) showed no trend. Univariate Mann-Kendall monotonic trend (R package, trend, [40]) were run on the individual station time series finding no trend in 28 of the 33 stations and of the five with p-value ≤0.05, all had negative trends.

The four plots of GAMs presented in Figures 6–9 and Table 3 were run with basis dimensions, k = 10. Increasing basis dimensions (up to 33) may explain as much as 50% of deviance but, in our opinion, over-explains the data. At k=10, GAMs of DOY onset and PAR explain 19.1% and 21.4% of deviance, respectively, the MR GAM, explains 13.3%, and the AR GAM explains 5.4%.

The three GAMs and SRMs shown in Figures 7–9 are more or less faithful representations of the GAM and SRM fit curves in Figure 6 but in mirror image. Nevertheless, time series autocorrelation analyses (R package, trend, [40]) of DOY onset failed to find correlations with AR at any lag other than +2. However, linear models using the means of DOY as predictor and MR and PAR as responsors produced R^2 of 0.431 and 0.418, respectively (p-value = <0.001). As have many other researchers, we found that early DOY onset produces more rain than late onsets [26,53,54].

The diagnostic bar charts, residual scatterplots, and QQ plots provided in Figures 6–9, all show the same left-skew, and slight to substantial departures from model expectation. Slight trends in the LRM lines for DOY onset, MR, and PAR, while presenting below threshold (<0.05) p-values, explain very little variance. Taken together however, they suggest the possibility that DOY onset is advancing in the year, MR is increasing, and PAR is increasing, implying a slight decrease in October-May rainfall.

Scatterplots of the time series of DOY onset, MR, AR, and PAR received during the monsoon suggest that, with respect to DOY onset, the sinusoidal troughs exhibit less variance than the crests. The uneven distribution of variance between the troughs and crests discussed in the previous section may be partly responsible for the low deviance and R^2 values produced in our GAM analysis and SRM fit.

The sinusoidal wave pattern seen in the scatterplots is reversed in the GAMs and SRMs of monsoon precipitation, annual precipitation, and the proportion of annual precipitation falling during the monsoon. Similar to the DOY onset waves, but in mirror image, these waves are broad in the troughs and narrow in the crests reflecting the predominance of late onsets and less rainfall. The

unbalanced distribution of variance coupled with the unequal spans of crests and troughs may explain the fit statistics observed in the GAMs and SRMs.

It is noteworthy that the NAME project previously referenced focused on the monsoon season of I June – 30 September 2004 [22], coinciding with an onset crest (Figure 7a) and monsoon precipitation trough (Figure 8a).

Table 4 is presented recognizing that the specific shapes of the curves rendered in the GAMs are partly subject to the choice of basis dimensions (k=10). Nevertheless, although period and amplitude estimates of the GAM curves (Figures 6–9) were used as starting points, each SRM required multiple iterations to arrive at the model selected and these match the GAMs relatively well. The DOY onset curve period, 3140 days (8.6 years) is calculated from the four distinct crests in the GAM curve (Figure 6), while the MR and AR and the PAR curves include only three crests in the 1990-2022 dataset, 3039, 3050, and 2969 days (8.3, 8.4, and 8.1 years) respectively. Note that the DOY onset wave period and the periods of the MR, AR, and PAR are not identical. The waves may be out of synchrony or, more likely, the data may not be sufficiently robust.

The sinusoid wave amplitudes (crest minus trough) produced by the GAMs are very substantial. The smallest amplitude in the DOY onset time series GAM is 14 days, the largest, 29 days or more than four weeks. The mean amplitudes of MR, AR, and PAR are 90 mm, 42 mm, and 25% respectively.

3.4. Previous Research

Climatologists have been researching the nature of the NAM for more than a century [55]. In assessing our results, we surveyed the relevant literature, a portion of which is listed in Table 5. The aims, priorities, and tools available to researchers over time have evolved from recognition, to characterization, investigations of origin, modelling, linkage to global systems, and, most recently, the future of the monsoon in a warming climate. These focus areas overlap and continue. Throughout this extensive history of research the identification and analysis of monsoon onset and retreat has relied on several approaches: single day rainfall thresholds, wind measurements, multi-day dewpoint and rainfall thresholds, combinations of climate variables, rainfall indices, and more.

Table 5 lists 21 NAM research contributions, only two of which, Ellis, et al. [56], García-Franco, et al. [57], were devoted to identifying dates of monsoon onset. Of the 20, two authors used multiple onset identifiers [27,58], 11 relied on variously constrained multi-day precipitation thresholds [25,26,54,59–67], five used abrupt or anomalous changes in rainfall amounts [27,53,58,68,69], three favored a multi-day dewpoint threshold [27,56,70], three prioritized change in wind direction [27,55,58], one employed multiple surface measurements [27], and one developed a novel wavelet transform procedure [57]. Each author chose a monsoon onset definition that would facilitate analysis or support a research goal as did we in choosing our own unique definition. Our interest lay in the need for desert plants at the tail end of a lengthy foresummer drought amid increasingly harsh temperatures to take advantage of the coming rains as quickly as possible. The ≥10 mm criterion was chosen as the least amount that would potentially trigger plant growth to support investigations of the phenology of desert plants, not monsoon season climatology. As it happened, our approach may have revealed an important pattern in DOY onset and precipitation that has so far escaped notice.

Table 5. List of monsoon onset papers, datasets, and approaches. Results of selected literature survey of synoptic NAM characteristics addressing onset, duration, or precipitation amounts, solely or in combination with other climatological investigations.

	Reference	Aim of study	Onset identifier(s)	Geography
1914	Huntington [55]	Describe monsoon climate of Ariz., New Mex.	Change in wind direction from westerly to southerly.	Ariz., New Mex.
1955	Bryson and Lowry [68]	Map shift in dominant air masses signaling monsoon season.	Sharp changes in Raininess Index.	Ariz.
1973	Brenner [27]	Describe antecedent monsoon climate of Ariz., investigate possible GoC connection.	Changes in several surface observations.	Ariz.

	Reference	Aim of study	Onset identifier(s)	Geography
1993	Douglas, et al. [58]	Describe synoptic climatology Mex., U.S. monsoon, identify moisture source(s).	Rainfall amounts and wind shifts.	Mex., SW U.S.
1997	Higgins, et al. [59]	Diagnose atmospheric conditions preceding monsoon onset.	Precip. index magnitude & duration, ⩽0.5 mm day⩾1 for 3 days.	Ariz., western New Mex.
1998	Higgins, et al. [60]	Extend earlier work, diagnose variability of Mex.-U.S. summer precip.	Precip. index magnitude & duration, ⩽0.5 mm day⩾1 for 3 days.	Ariz., western New Mex.
1999	Higgins, et al. [61]	Extend earlier work, identify factors influencing variability.	Varies by region; precip. index magnitude & duration, ⩽0.5-2 mm day⩾1 for 3-5 days.	Ariz., western New Mex., SW Mex.
2002	Mitchell, et al. [62]	Onset & evolution of monsoon rainfall related to GOC SSTs.	Varies by region; precip. index magnitude & duration, ⩽0.5-2 mm day⩾1 for 3-5 days..	GoC, Ariz., New Mex.
2004	Ellis, et al. [56]	Develop regional criteria for monsoon onset.	Mean daily dew-point threshold 12.2º or 12.8º for 3 days.	SW U.S.
2007	Grantz, et al. [69]	NAM timing, rainfall amount, large-scale trends drivers.	Percentile of monsoon precip. threshold.	Ariz., New Mex.
2008	Liebmann, et al. [53]	Monsoon onset dates Mex. & U.S. climatology variability, season length, rate, SST topography influences.	Anomalous rainfall accumulation.	Mex., SW U.S.
2009	Turrent and Cavazos [63]	Clarify monsoon forcing with land-sea thermal flux and influence on onset.	First 5-day period mean core region precip. >1 mm.	NW Mex.
2011	Crimmins, et al. [70]	Relate summer flowering onset to monsoon climatological events.	3-day mean daily dewpoint threshold at TUS.	Finger Rock Canyon, Pima Co., Ariz.
2012	Arias, et al. [64]	Determine multidecadal variations in monsoon seasonality & strength.	Pentad after which the rain rate > than annual mean rain rate in 6 of 8 preceding pentads and after which rain rate > than annual mean in 6 of 8 pentads.	NW Mex.
2015	Arias, et al. [25]	Investigate climate dynamics influencing variability of NAM and SAM.	Pentad after which the rain rate > than annual mean rain rate in 6 of 8 preceding pentads and after which rain rate > than annual mean in 6 of 8 pentads.	North America, South America
2017	Meyer and Jin [54]	Correct regional and global models for projected future climate effects on monsoon dynamics.	First occurrence after 1 May with three consecutive days with at least 0.5 mm day−1.	SW U.S., Mex.
2021	García-Franco, et al. [57]	Introduce new onset identifier.	Wavelet transform (maximum sum of wavelet coefficients) on precip. time series.	Mex., India
2021	Fonseca-Hernandez, et al. [65]	Analyze mixing mechanisms responsible for temporal and spatial variations of GoC boundary layer during NAM onset.	First day first sequence of five consecutive days mean precip. rate =/> 2 mm/day.	NW Mex.
2021	Ashfaq, et al. [26]	Construct regional climate model of monsoon change with increased greenhouse gas forcing.	Pentad after minimum seasonality of precip. value, similar to Bombardi and Carvalho [74].	Global monsoon domains
2024	Duan, et al. [67]	Identify and analyze NAM extreme events.	First 1 mm/day for 5 days after 1 June.	GoC and surrounding lands

With one exception ([48]) among all research studies cited in this paper, analyses were performed using summarized data, usually by extracting and analyzing mean values, often in gridded datasets or compiled as means of variables from terrestrial stations. This was presumably done to avoid violations of independence of observations. Our dataset was extracted from terrestrial sensors and the main analysis was performed with daily rainfall data (although we report mean

values) from which we extracted single-day yearly onsets for each station for each year 1990-2022. As reported above, we tested the assumption of independence in our DOY onset variable station means using the ESRI ArcGIS spatial autocorrelation tool [36] and found the resulting Moran's I indicated not different from random. The sinusoidal wave pattern observed in the scatterplot is likely to be real and worthy of further investigation.

3.5. Saguaro Phenology

The research described in the previous section suggests sinusoidal waves in timing of DOY onset, MR, AR, and PAR from 1990-2022. It is unknown whether that pattern extends back in time to any extent. Saguaros are very long-lived, up to 250 years [71], and it would be very interesting to know whether, or to what degree saguaros have adapted to regular cycles of abundance and shortage. Even if the sinusoidal wave only appeared *de novo* in 1990, saguaro reproduction, which as we have noted, is highly dependent on the monsoon as it is now. As noted above, the variations in DOY onset and MR reported here are quite substantial. The sinusoidal waves have amplitudes of up to 30 days and nearly 100 mm, respectively.

The possible effect of changes in DOY onset timing and monsoon precipitation, over time on saguaro phenology bears further research in light of predicted changes in saguaro distribution under the influence of anthropogenic climate change. Albuquerque, et al. [72] predict loss of currently occupied saguaro habitat in the next half century and Renzi, et al. [7], using saguaro phenological data from a population of 151 saguaros monitored from 2004-2013 found that saguaro flowering was increasingly delayed while the number of flowers produced declined overall. These reports do not, at least on the surface, appear to reflect any relationship with the sinusoidal waves suggested in our data. Attempts have been made to analyze multi-decadal patterns of recruitment and growth [73], but it is highly unlikely that the very long-lived saguaro cactus would adapt to this short-period cyclic climatology.

4. Conclusions

The dependency of saguaro population biology on monsoon precipitation prompted us to gather precipitation data from 33 weather stations in south-central Arizona and identify the date of monsoon onset at each station from 1990-2022. In the near future we plan to update the saguaro phenology dataset in Renzi, et al. [7] to address this question.

The results reported here suggest that the DOY onset time series exhibits a sinusoidal wave fit to a GAM with period of 8.6 years and mean crest-trough amplitude of 20 days. The relationship is weak, explaining only 19.1% of deviance. We suggest some preliminary explanations for greater data variance from troughs to crests.

We report interesting and, we think, very important patterns in selected NAM characteristics. We can offer no plausible explanation except to suggest interplay between sub-global climate systems that leads to spatially recurring systems. Before the drivers of the monsoon patterns suggested here can be elucidated much work remains to be done to establish: (1) whether, or which, of the patterns, especially timing of DOY onset, are real, (2) what is the spatial extent of the patterns, (3) how long before 1990 do the patterns extend. and (4) can we create models sufficiently robust to support forecasting?

It is hoped that future work on the DOY onset features found in our data will be explained and clarified with greater resolution than is presented here. We look forward to insights into the nature of the sinusoidal wave in the DOY onset data, clarification of the geospatial characteristics of DOY onset timing, and we hope that some progress may be made in extending analysis of DOY onset to substantially before 1990.

Conflicts of Interest declaration: The authors declare that they have no affiliations with or involvement in any organization or entity with any financial interest in the subject matter or materials discussed in this manuscript.

References

1. Conn, J.; Snyder-Conn, E. The relationship of the rock outcrop microhabitat to germination, water relations, and phenology of Erythrina flabelliformis (Fabaceae) in southern Arizona. *Southwestern Naturalist* 1981, 443-451.

2. Bowers, J. E.; Dimmitt, M. A. Flowering phenology of six woody plants in the northern Sonoran Desert. *Bulletin of the Torrey Botanical Club* 1994, 215-229.

3. Bustamante, E.; Búrquez, A. Effects of Plant Size and Weather on the Flowering Phenology of the Organ Pipe Cactus (Stenocereus thurberi). *Annals of Botany* 2008, *102* (6), 1019-1030. DOI: 10.1093/aob/mcn194 (acccessed 2023-12-05T22:31:31).

4. Fisogni, A.; De Manincor, N.; Bertelsen, C. D.; Rafferty, N. E. Long-term changes in flowering synchrony reflect climatic changes across an elevational gradient. *Ecography* 2022, *2022* (2). DOI: 10.1111/ecog.06050 (acccessed 2023-12-05T22:44:28).

5. Bowers, J. E.; Turner, R. M. The influence of climatic variability on local population dynamics of Cercidium microphyllum (foothill paloverde). *Oecologia* 2002, *130* (1), 105-113. DOI: 10.1007/s004420100779 (acccessed 2023-12-05T22:50:01).

6. Zachmann, L. J.; Wiens, J. F.; Franklin, K.; Crausbay, S. D.; Landau, V. A.; Munson, S. M. Dominant Sonoran Desert Plant Species Have Divergent Phenological Responses to Climate Change. *Madroño* 2021, *68* (4). DOI: 10.3120/0024-9637-68.4.473 (acccessed 2023-12-05T22:57:10).

7. Renzi, J. J.; Peachey, W. D.; Gerst, K. L. A decade of flowering phenology of the keystone saguaro cactus (<i>Carnegiea gigantea</i>). *American Journal of Botany* 2019, *106* (2), 199-210. DOI: 10.1002/ajb2.1231 (acccessed 2023-12-05T22:34:16).

8. Bowers, J. E. Environmental determinants of flowering date in the columnar cactus Carnegiea gigantea in the northern Sonoran Desert. *Madrono* 1996, 69-84.

9. Foley, T.; Swann, D.; Sotelo, G.; Perkins, N. Is the timing of saguaro flowering changing? Using citizen science to understand changes in saguaro phenology. Western National Parks Association, Tucson, Arizona: 2021; p 12.

10. Steenbergh, W. F.; Lowe, C. H. *Ecology of the Saguaro: II, Reproduction, Germination, Establishment, Growth, and Survival of the Young Plant: Warren F. Steenbergh & Charles H. Lowe*; Department of the Interior, National Park Service, 1977.

11. Bowers, J. E. Regeneration of triangle-leaf bursage (Ambrosia deltoidea: Asteraceae): germination behavior and persistent seed bank. *The Southwestern Naturalist* 2002, *47* (3), 449-453.

12. Bowers, J. E. New evidence for persistent or transient seed banks in three Sonoran Desert cacti. *The Southwestern Naturalist* 2005, *50* (4), 482-487.

13. Stella, J. C.; Battles, J. J.; Orr, B. K.; Mcbride, J. R. Synchrony of Seed Dispersal, Hydrology and Local Climate in a Semi-arid River Reach in California. *Ecosystems* 2006, *9* (7), 1200-1214. DOI: 10.1007/s10021-005-0138-y (acccessed 2023-12-06T01:31:20).

14. Crimmins, T. M.; Bertelsen, C. D.; Crimmins, M. A. Within-season flowering interruptions are common in the water-limited Sky Islands. *International Journal of Biometeorology* 2014, *58* (4), 419-426. DOI: 10.1007/s00484-013-0745-9 (acccessed 2023-12-06T01:27:43).

15. Meyer, S. E.; Pendleton, B. K. Evolutionary drivers of mast-seeding in a long-lived desert shrub. *American Journal of Botany* 2015, *102* (10), 1666-1675. DOI: 10.3732/ajb.1500209 (acccessed 2023-12-06T01:23:20).

16. Prevéy, J. S.; Vitasse, Y.; Fu, Y. Editorial: Experimental Manipulations to Predict Future Plant Phenology. *Frontiers in Plant Science* 2021, *11*. DOI: 10.3389/fpls.2020.637156 (acccessed 2023-12-06T01:36:20).

17. Vera, C.; Higgins, W.; Amador, J.; Ambrizzi, T.; Garreaud, R.; Gochis, D.; Gutzler, D.; Lettenmaier, D.; Marengo, J.; Mechoso, C. R.; et al. Toward a Unified View of the American Monsoon Systems. *Journal of Climate* 2006, *19* (20), 4977-5000. DOI: 10.1175/jcli3896.1 (acccessed 2023-12-13T22:05:58).

18. Gadgil, S. The monsoon system: Land–sea breeze or the ITCZ? *Journal of Earth System Science* 2018, *127* (1). DOI: 10.1007/s12040-017-0916-x (acccessed 2023-12-05T20:22:01).

19. Biasutti, M.; Voigt, A.; Boos, W. R.; Braconnot, P.; Hargreaves, J. C.; Harrison, S. P.; Kang, S. M.; Mapes, B. E.; Scheff, J.; Schumacher, C.; et al. Global energetics and local physics as drivers of past, present and future monsoons. *Nature Geoscience* 2018, *11* (6), 392-400. DOI: 10.1038/s41561-018-0137-1 (acccessed 2023-12-05T20:10:02).

20. Geen, R.; Bordoni, S.; Battisti, D. S.; Hui, K. Monsoons, ITCZs, and the Concept of the Global Monsoon. *Reviews of Geophysics* 2020, *58* (4). DOI: 10.1029/2020rg000700 (acccessed 2023-12-05T19:28:02).

21. Wang, B.; Ding, Q. Global monsoon: Dominant mode of annual variation in the tropics. *Dynamics of Atmospheres and Oceans* 2008, *44* (3-4), 165-183.

22. Higgins, W.; Gochis, D. Synthesis of Results from the North American Monsoon Experiment (NAME) Process Study. *Journal of Climate* 2007, *20* (9), 1601-1607. DOI: 10.1175/jcli4081.1 (acccessed 2023-12-05T21:19:02).

23. Mo, K.; Higgins, R. W. Relationships between Sea Surface Temperatures in the Gulf of California and Surge Events. *Journal of Climate* 2008, *21* (17), 4312-4325. DOI: 10.1175/2008jcli2113.1 (acccessed 2023-12-05T21:42:10).

24. Zuidema, P.; Fairall, C.; Hartten, L. M.; Hare, J. E.; Wolfe, D. On Air–Sea Interaction at the Mouth of the Gulf of California. *Journal of Climate* 2007, *20* (9), 1649-1661. DOI: 10.1175/jcli4089.1 (acccessed 2023-12-05T21:46:50).

25. Arias, P. A.; Fu, R.; Vera, C.; Rojas, M. A correlated shortening of the North and South American monsoon seasons in the past few decades. *Climate Dynamics* 2015, *45* (11-12), 3183-3203. DOI: 10.1007/s00382-015-2533-1 (acccessed 2023-12-05T21:51:37).

26. Ashfaq, M.; Cavazos, T.; Reboita, M. S.; Torres-Alavez, J. A.; Im, E.-S.; Olusegun, C. F.; Alves, L.; Key, K.; Adeniyi, M. O.; Tall, M. Robust late twenty-first century shift in the regional monsoons in RegCM-CORDEX simulations. *Climate Dynamics* 2021, *57*, 1463-1488.

27. Brenner, I. S. *A surge of maritime tropical air--Gulf of California to the southwestern United States*; US Department of Commerce, National Oceanic and Atmospheric Administration …, 1973.

28. Carleton, A. Synoptic and satellite aspects of the southwestern US summer 'monsoon'. *International Journal of Climatology* 1985, *5* (4), 389-402.

29. Bombardi, R. J.; Moron, V.; Goodnight, J. S. Detection, variability, and predictability of monsoon onset and withdrawal dates: A review. *International Journal of Climatology* 2020, *40* (2), 641-667.

30. Bowers, J. E.; Turner, R. M.; Burgess, T. L. Temporal and spatial patterns in emergence and early survival of perennial plants in the Sonoran Desert. *Plant Ecology (formerly Vegetatio)* 2004, *172* (1), 107-119. DOI: 10.1023/b:vege.0000026026.34760.1b (acccessed 2023-12-06T04:09:51).

31. Pima County Regional Flood Control District. *PCRFCD ALERT Google Data Display Map*. 2023. https://alertmap.rfcd.pima.gov/gmap/gmap.html (accessed 2023 9/23/2023).

32. Global Historical Climatology Network - Daily (GHCN-Daily), Version 3. NOAA National Climatic Data Center. https://www.ncei.noaa.gov/cdo-web/search?datasetid=GHCND (accessed 9/23/2023).

33. Menne, M. J.; Durre, I.; Vose, R. S.; Gleason, B. E.; Houston, T. G. An Overview of the Global Historical Climatology Network-Daily Database. *J. Atmos. Oceanic Technol.* 2012, *29*, 897-910. DOI: 10.1175/JTECH-D-11-00103.1.

34. RAWS USA Climate Archive. Western Regional Climate Center. https://raws.dri.edu/wraws/ (accessed 9/23/2023).

35. Thorsen, S. *Solstices & Equinoxes for Tucson (1990-2022)*. 2024. https://www.timeanddate.com/calendar/seasons.html?n=393 (accessed 2023 9/23/2023).

36. ESRI. *Spatial Autocorrelation Tool, ArcGIS Pro 3.2*. Environmental Systems Research Institute, 2023. https://pro.arcgis.com/en/pro-app/latest/tool-reference/spatial-statistics/spatial-autocorrelation.htm (accessed 2023 9/23/2023).

37. Moritz, S.; Bartz-Beielstein, T. imputeTS: Time Series Missing Value Imputation in R. *The   R Journal* 2017, *9* (1), 207-218. DOI: https://doi.org/10.32614/RJ-2017-009.

38. R Core Team.*R: A language and environment for statistical computing*; R Foundation for Statistical Computing: Vienna, Austria, 2022. https://www.R-project.org/ (accessed 9/23/2023).

39. Hyndman, R.; Athanasopoulos, G.; Bergmeir, C.; Caceres, G.; Chhay, L.; O'Hara-Wild, M.; Petropoulos, F.; Razbash, S.; Wang, E.; Yasmeen, F.*forecast: Forecasting functions for time series and linear models*; 2024. https://pkg.robjhyndman.com/forecast/ (accessed.

40. Pohlert, T.*trend: Non-Parametric Trend Tests and Change-Point Detection*; 2023. https://CRAN.R-project.org/package=trend (accessed.

41. Wood, S. N. Generalized Additive Models. 2017. DOI: 10.1201/9781315370279 (acccessed 2024-04-07T05:42:05).

42. Underwood, F. M. Describing long-term trends in precipitation using generalized additive models. *Journal of hydrology* 2009, *364* (3-4), 285-297.

43. Haruna, A.; Blanchet, J.; Favre, A.-C. Performance-based comparison of regionalization methods to improve the at-site estimates of daily precipitation. *Hydrology and Earth System Sciences* 2022, *26* (10), 2797-2811. DOI: 10.5194/hess-26-2797-2022 (acccessed 2024-04-09T03:50:38).

44. Wood, S. N. Fast stable restricted maximum likelihood and marginal likelihood estimation of semiparametric generalized linear models. *Journal of the Royal Statistical Society Series B: Statistical Methodology* 2011, *73* (1), 3-36.

45. Mathworks, I.*Symbolic Math Toolbox*; 2024. https://www.mathworks.com/help/symbolic/ (accessed.

46. Sheppard, P. R.; Comrie, A. C.; Packin, G. D.; Angersbach, K.; Hughes, M. K. The climate of the US Southwest. *Climate Research* 2002, *21* (3), 219-238.

47. Hughes, M.; Mahoney, K. M.; Neiman, P. J.; Moore, B. J.; Alexander, M.; Ralph, F. M. The Landfall and Inland Penetration of a Flood-Producing Atmospheric River in Arizona. Part II: Sensitivity of Modeled Precipitation to Terrain Height and Atmospheric River Orientation. *Journal of Hydrometeorology* 2014, *15* (5), 1954-1974. DOI: 10.1175/jhm-d-13-0176.1 (acccessed 2023-12-10T15:03:40).

48. Petrie, M.; Collins, S.; Gutzler, D.; Moore, D. Regional trends and local variability in monsoon precipitation in the northern Chihuahuan Desert, USA. *Journal of Arid Environments* 2014, *103*, 63-70.

49. Gochis, D. J.; Jimenez, A.; Watts, C. J.; Garatuza-Payan, J.; Shuttleworth, W. J. Analysis of 2002 and 2003 Warm-Season Precipitation from the North American Monsoon Experiment Event Rain Gauge Network. *Monthly Weather Review* 2004, *132* (12), 2938-2953. DOI: 10.1175/mwr2838.1 (acccessed 2023-12-10T17:42:17).

50. Gebremichael, M.; Vivoni, E. R.; Watts, C. J.; Rodríguez, J. C. Submesoscale Spatiotemporal Variability of North American Monsoon Rainfall over Complex Terrain. *Journal of Climate* 2007, *20* (9), 1751-1773. DOI: 10.1175/jcli4093.1 (acccessed 2025-02-22T22:43:02).

51. Mascaro, G.; Vivoni, E. R.; Gochis, D. J.; Watts, C. J.; Rodriguez, J. C. Temporal Downscaling and Statistical Analysis of Rainfall across a Topographic Transect in Northwest Mexico. *Journal of Applied Meteorology and Climatology* 2014, *53* (4), 910-927. DOI: 10.1175/jamc-d-13-0330.1 (acccessed 2025-02-22T14:38:40).

52. McDonald, J. E. *Variability of precipitation in an arid region: A survey of characteristics for Arizona*; Institute of Atmospheric Physics, University of Arizona (Tucson, AZ), 1956.

53. Liebmann, B.; Bladé, I.; Bond, N. A.; Gochis, D.; Allured, D.; Bates, G. T. Characteristics of North American Summertime Rainfall with Emphasis on the Monsoon. *Journal of Climate* 2008, *21* (6), 1277-1294. DOI: 10.1175/2007jcli1762.1 (acccessed 2025-02-07T22:03:23).

54. Meyer, J. D. D.; Jin, J. The response of future projections of the North American monsoon when combining dynamical downscaling and bias correction of CCSM4 output. *Climate Dynamics* 2017, *49* (1-2), 433-447. DOI: 10.1007/s00382-016-3352-8 (acccessed 2023-12-14T15:38:19).

55. Huntington, E. *The climatic factor as illustrated in arid America*; Carnegie institution of Washington, 1914.

56. Ellis, A. W.; Saffell, E. M.; Hawkins, T. W. A method for defining monsoon onset and demise in the southwestern USA. *International Journal of Climatology: A Journal of the Royal Meteorological Society* 2004, *24* (2), 247-265.

57. García-Franco, J. L.; Gray, L. J.; Osprey, S. The American monsoon system in HadGEM3 and UKESM1. *Weather and Climate Dynamics* 2020, *1* (2), 349-371. DOI: 10.5194/wcd-1-349-2020 (acccessed 2023-12-08T01:59:48).

58. Douglas, M. W.; Maddox, R. A.; Howard, K.; Reyes, S. The mexican monsoon. *Journal of Climate* 1993, *6* (8), 1665-1677.

59. Higgins, R.; Yao, Y.; Wang, X. Influence of the North American monsoon system on the US summer precipitation regime. *Journal of climate* 1997, *10* (10), 2600-2622.

60. Higgins, R.; Mo, K.; Yao, Y. Interannual variability of the US summer precipitation regime with emphasis on the southwestern monsoon. *Journal of Climate* 1998, *11* (10), 2582-2606.

61. Higgins, R. W.; Chen, Y.; Douglas, A. V. Interannual variability of the North American Warm Season Precipitation Regime. *Journal of Climate* 1999, *12*, 653-680. (acccessed 2023-12-05T15:29:58).

62. Mitchell, D. L.; Ivanova, D.; Rabin, R.; Brown, T. J.; Redmond, K. Gulf of California sea surface temperatures and the North American monsoon: Mechanistic implications from observations. *Journal of Climate* 2002, *15* (17), 2261-2281.

63. Turrent, C.; Cavazos, T. Role of the land-sea thermal contrast in the interannual modulation of the North American Monsoon. *Geophysical Research Letters* 2009, *36* (2), n/a-n/a. DOI: 10.1029/2008gl036299 (acccessed 2025-02-07T22:19:03).

64. Arias, P. A.; Fu, R.; Mo, K. C. Decadal Variation of Rainfall Seasonality in the North American Monsoon Region and Its Potential Causes. *Journal of Climate* 2012, *25* (12), 4258-4274. DOI: 10.1175/jcli-d-11-00140.1 (acccessed 2023-12-07T21:48:53).

65. Fonseca-Hernandez, M.; Turrent, C.; Mayor, Y. G.; Tereshchenko, I. Using Observational and Reanalysis Data to Explore the Southern Gulf of California Boundary Layer During the North American Monsoon Onset. *Journal of Geophysical Research: Atmospheres* 2021, *126* (7). DOI: 10.1029/2020jd033508 (acccessed 2024-11-12T23:10:16).

66. Carleton, A. M.; Carpenter, D. A.; Weser, P. J. Mechanisms of interannual variability of the southwest United States summer rainfall maximum. *Journal of Climate* 1990, *3* (9), 999-1015.

67. Duan, S.; Ullrich, P.; Boos, W. R. Meteorological Drivers of North American Monsoon Extreme Precipitation Events. *Journal of Geophysical Research: Atmospheres* 2024, *129* (13). DOI: 10.1029/2023jd040535 (acccessed 2025-01-31T23:40:07).

68. Bryson, R. A.; Lowry, W. P. Synoptic Climatology of the Arizona Summer Precipitation Singularity *, #. *Bulletin of the American Meteorological Society* 1955, *36* (7), 329-339. DOI: 10.1175/1520-0477-36.7.329 (acccessed 2025-02-10T23:03:30).

69. Grantz, K.; Rajagopalan, B.; Clark, M.; Zagona, E. Seasonal Shifts in the North American Monsoon. *Journal of Climate* 2007, *20* (9), 1923-1935. DOI: 10.1175/jcli4091.1 (acccessed 2025-02-07T22:09:27).

70. Crimmins, T. M.; Crimmins, M. A.; Bertelsen, C. D. Onset of summer flowering in a 'Sky Island' is driven by monsoon moisture. *New Phytologist* 2011, *191* (2), 468-479. DOI: 10.1111/j.1469-8137.2011.03705.x (acccessed 2025-02-08T14:45:44).

71. Drezner, T. D. How long does the giant saguaro live? Life, death and reproduction in the desert. *Journal of Arid Environments* 2014, *104*, 34-37.

72. Albuquerque, F.; Benito, B.; Rodriguez, M. Á. M.; Gray, C. Potential changes in the distribution of Carnegiea gigantea under future scenarios. *PeerJ* 2018, *6*, e5623.

73. Félix-Burruel, R. E.; Larios, E.; González, E. J.; Búrquez, A. Episodic recruitment in the saguaro cactus is driven by multidecadal periodicities. *Ecology* 2021, *102* (10), e03458.

74. Bombardi, R. J.; Carvalho, L. M. V. IPCC global coupled model simulations of the South America monsoon system. *Climate Dynamics* 2009, *33* (7-8), 893-916. DOI: 10.1007/s00382-008-0488-1 (acccessed 2025-02-10T22:18:45).